Characterization of Novel Fluorescent Bile Salt Derivatives for Studying Human Bile Salt and Organic Anion Transporters[S]

Michele Leuenberger,[1] Stephanie Häusler,[1] Vera Höhn, Adriana Euler, Bruno Stieger, and ⓘ Martin Lochner

Institute of Biochemistry and Molecular Medicine, University of Bern, Bern, Switzerland (M.Le., M.Lo.); Department of Clinical Pharmacology and Toxicology, University Hospital Zürich, Zürich, Switzerland (S.H., V.H., A.E., B.S.); and Swiss National Center of Competence in Research, NCCR TransCure, Bern, Switzerland (M.Le., S.H., A.E., B.S., M.Lo.)

ABSTRACT

Bile salts, such as cholate, glycocholate, taurocholate, and glycochenodeoxycholate, are taken up from the portal blood into hepatocytes via transporters, such as the Na+-taurocholate–cotransporting polypeptide (NTCP) and organic anion–transporting polypeptides (OATPs). These bile salts are later secreted into bile across the canalicular membrane, which is facilitated by the bile salt export pump (BSEP). Apart from bile salt transport, some of these proteins (e.g., OATPs) are also key transporters for drug uptake into hepatocytes. In vivo studies of transporter function in patients by using tracer compounds have emerged as an important diagnostic tool to complement classic liver parameter measurements by determining dynamic liver function both for diagnosis and monitoring progression or improvement of liver diseases. Such approaches include use of radioactively labeled bile salts (e.g., for positron emission tomography) and fluorescent bile salt derivatives or dyes (e.g., indocyanine green). To expand the list of liver function markers, we synthesized fluorescent derivatives of cholic and chenodeoxycholic acid by conjugating small organic dyes to the bile acid side chain. These novel fluorescent probes were able to block substrate transport in a concentration-dependent manner of NTCP, OATP1B1, OATP1B3, OATP2B1, BSEP, and intestinal apical sodium-dependent bile salt transporter (ASBT). Whereas the fluorescent bile acid derivatives themselves were transported across the membrane by OATP1B1, OATP1B3, and OATP2B1, they were not transport substrates for NTCP, ASBT, BSEP, and multidrug resistance-related protein 2. Accordingly, these novel fluorescent bile acid probes can potentially be used as imaging agents to monitor the function of OATPs.

SIGNIFICANCE STATEMENT

Synthetic modification of common bile acids by attachment of small organic fluorescent dyes to the bile acid side chain resulted in bright, fluorescent probes that interact with hepatic and intestinal organic anion [organic anion–transporting poly-peptide (OATP) 1B1, OATP1B3, OATP2B1], bile salt uptake (Na+-taurocholate–cotransporting polypeptide, apical sodium-dependent bile salt transporter), and bile salt efflux (bile salt export pump, multidrug resistance-related protein 2) transporters. Although the fluorescent bile salt derivatives are taken up into cells via the OATPs, the efflux transporters do not transport any of them but one.

Introduction

Bile formation is one of several important liver functions (Stieger, 2011). The liver is also a second barrier for preventing the entry of harmful substances into the body via the oral route because of its role in detoxification (Corsini and Bortolini, 2013; Selvapatt et al., 2014). Consequently, the liver is constantly at risk of insults by xenobiotics, which may lead to liver injury in susceptible patients (Corsini and Bortolini, 2013).

The major constituents of bile are bile salts (BSs), which are organic anions like conjugates of bilirubin and lipids (Esteller, 2008). BSs are absorbed from the portal blood into hepatocytes from which they are secreted across the canalicular membrane into bile draining into the small intestine. In the intestine, BSs are almost quantitatively absorbed and transported back into the liver by the portal vein, where their journey starts again. The transport systems involved in hepatocellular handling of

ABBREVIATIONS: abs, absorption; Acen, acetyl ethylenediamine; ASBT, apical sodium-dependent bile salt transporter; BA, bile acid; br, broad peak; BS, bile salt; BSEP, bile salt export pump; CDCen, (2-aminoethyl)chenodeoxycholic amide; Cen, (2-aminoethyl)cholic amide; d, doublet; DCM, dichloromethane; DMF, *N,N*-dimethylformamide; DNS, Dansyl, 5-(dimethylamino)naphthalene-1-sulfonamide; em, emission; EtOAc, ethyl acetate; ex, excitation; eq., equivalent; FCS, fetal calf serum; Fluo, fluorescence; HRMS, high-resolution mass spectra; LC, liquid chromatography; m, multipletMeOH methanol *m/z* mass-to-charge ratio; MRP, multidrug resistance-related protein; MS, mass spectrometry; NBD, 4-nitrobenzo[c][1,2,5]oxadiazole; NTCP, Na+-taurocholate–cotransporting polypeptide; OATP, organic anion–transporting polypeptide; OST, organic solute transporter; PB, Pacific Blue, 6,8-difluoro-7-hydroxy-2-oxo-2*H*-chromene-3-carboxamide; q, quartet; s, singlet; t, triplet; TLC, thin-layer chromatography; WT, wild type.

bile acids (BAs) and BSs are known (Stieger, 2011; Pollheimer et al., 2014) and include for the uptake from the blood plasma the Na$^+$-taurocholate–cotransporting polypeptide (NTCP) and the organic anion–transporting polypeptides (OATPs) OATP1B1, OATP1B3, and OATP2B1. Efflux of BS from hepatocytes into bile is mediated by the BS export pump (BSEP). In the intestine, BSs are reclaimed by the apical sodium-dependent BS transporter (ASBT) in the apical membrane of enterocytes in the distal ileum. Export from enterocytes is accomplished through the basolateral membrane by the organic solute transporter (OST) α/OSTβ (Dawson and Karpen, 2015). In hepatocytes, MRP3, MRP4, and OSTα/OSTβ are expressed at the basolateral membrane and may act as salvage transporters for BS in cholestatic conditions (Halilbasic et al., 2013).

BS export by BSEP constitutes the rate-limiting step of hepatocellular BS flux. Inherited or acquired impairment of BSEP function may lead to liver disease (Aithal et al., 2011; Bull and Thompson, 2018). The substrate specificity of BSEP is restricted with very few exceptions to BS (Stieger, 2011). Similarly, the main substrates for NTCP and ASBT are BSs (Anwer and Stieger, 2014). In addition to contributing to BA uptake into hepatocytes, OATPs have a broad substrate specificity and are key transporters for drug uptake (Hagenbuch and Stieger, 2013).

Measurements of so-called liver parameters are an important part of diagnosing liver disease. These parameters often only allow indirect conclusions on liver function. For example, serum-bilirubin levels give indirect information on the uptake, metabolic, and excretory/secretory functions of the liver (Hoekstra et al., 2013). To obtain more direct functional (or dynamic) information on the liver, in vivo determination of hepatocellular transporter function has become an active area of translational research (Stieger et al., 2012). Recent data show, for instance, that in vivo determination of liver function by monitoring hepatobiliary transport of ^{99m}Tc-mebrofenin with scintigraphy improves the outcome of risk assessment for patients needing major liver resection (Cieslak et al., 2016).

It was recognized that BSs are elevated in plasma in patients with liver disease (Frosch and Wagener, 1967), and it was later demonstrated that in such patients the clearance of glycocholate is reduced (LaRusso et al., 1975) and that the clearances of taurocholate and indocyanine green correlate well (Paumgartner et al., 1979). However, because of the endogenous BS pool, clearance measurements require radioactive BS (LaRusso et al., 1975). BS transport in vivo is currently explored by positron emission tomography, wherein hepatic transport of a BA derivative can be monitored in healthy individuals and patients (Cieslak et al., 2016; Kjærgaard et al., 2021). Such techniques expose patients to internal radiation and require complex methodologies. An alternate method is using fluorescence measurements. Spectrophotometric determination of indocyanine green clearance is routinely used to assess liver function (Stieger et al., 2012) and can also be performed transcutaneously, allowing continuous monitoring of liver function (Sakka, 2018). A pilot study demonstrated that the plasma clearance of the fluorescent BS cholyl-lysyl-fluorescein is reduced in patients with liver cirrhosis compared with healthy controls (Milkiewicz et al., 2000). However, this BS derivative is neither a substrate of NTCP nor BSEP (de Waart et al., 2010). Other fluorescein-BS

conjugates like CGamF (Holzinger et al., 1997, 1998) and, more recently, ^{18}F-labeled BS derivatives (Testa et al., 2017) have been studied as potential tracers of hepatic transporters in rat.

In this work, we aimed to test novel fluorescent BAs as potential liver function indicators. We synthesized novel fluorescent BA conjugates by modifying the side chain and tested their interaction with BS transporters using in vitro test systems. Although the new fluorescent BS conjugates inhibited all tested transporters except MRP2, these conjugates were substrates to OATPs only, albeit to different extents.

Materials and Methods

Materials Transporter Biology

Radiolabeled [6,7-^{3}H(N)]-estradiol 17β-D-glucuronide, [6,7-^{3}H(N)]-estrone sulfate, [^{3}H(G)]-taurocholic acid, and scintillation cocktail Ultima Gold were obtained from PerkinElmer (Schwerzenbach, Switzerland). [6,7-^{3}H(N)]-estradiol 17β-D-glucuronide and taurocholic acid sodium salt were from Sigma-Aldrich (St. Louis, MO). Cell Culture Material: CHO-Flp-In cells and LipofectAMINE 2000 were from Invitrogen (Carlsbad, CA). The baculovirus-expressing MRP2 (de Waart et al., 2010) was the generous gift of Drs. Paulusma and Oude Elferink, Academic Medical Center, Amsterdam (The Netherlands).

Transporter Expression Systems

CHO cells stably expressing OATP1B1, OATP1B3, or OATP2B1 were characterized by Treiber et al. (2007) and Gui et al. (2008). The cells were maintained in Dulbecco's modified Eagle's medium supplemented with 10% (v/v) fetal calf serum (FCS): 50 μg/ml L-proline, 100 U/100 μg per ml penicillin/streptomycin, and 500 μg/ml geneticin sulfate for transfected cells.

The generation of CHO Flp-In cells stably expressing NTCP was reported by de Waart et al. (2010). The CHO cell line stably expressing ASBT was established as follows: CHO Flp-In cells were cotransfected with pcDNATM5/FRT-hASBT (Zhao et al., 2015) and pOG44 (ratio 1:9) using the LipofectAMINE 2000 method according to the manufacturer's protocol. Cells were selected in medium supplemented with 500 μg/ml hygromycin B, and single clones were obtained by the use of cloning cylinders. The clones were assessed by determination of mRNA expression levels and taurocholate transport activity. CHO Flp-In cells were cultured in HAM-F12 medium enriched with 10% (v/v) FCS, 1 mM L-glutamine, 100 U/100 μg per ml penicillin/streptomycin, 100 μg/ml Zeocin (control cells), or 500 μg/ml hygromycin B (transfected cells).

The efflux transporter BSEP (Noé et al., 2002) and MRP2 (de Waart et al., 2006) were expressed with the baculovirus system in Sf21 cells, and membrane vesicles were isolated as described (Gerloff et al., 1998). Sf21 cells were grown Grace's insect medium containing 10% (v/v) heat-inactivated FCS and penicillin/streptomycin at 100 U/100 μg per ml.

Transport Experiments

Cell culture and transport experiments with radioactively labeled substrates were performed as detailed by Wlcek et al. (2013). Prior to transport experiments, the cells were cultured for 24 hours in the respective medium containing 5 mM sodium butyrate to increase protein expression of the transporters (Palermo et al., 1991). The following substrate concentrations were used for transport experiments with radioactively labeled substrates: 1 μM taurocholate for ASBT, 5 μM taurocholate for NTCP, 1 μM estrone-3-sulfate for OATP1B1 and OATP2B1, 5 μM taurocholate for OATP1B3, 10 μM estradiol 17β-D-glucuronide for MRP2, and 2 μM taurocholate for

BSEP. For the kinetic characterization of the established ASBT cell line, initial uptake rates were first determined (unpublished data). To test fluorescent compounds as substrates, they were in all experiments used at a concentration of 5 μM. In case of fluorescently labeled bile salts, the cells were solubilized after the transport experiment for at least 30 minutes with 1 ml of 1% (w/v) Triton X-100, and fluorescence was determined in a PerkinElmer LS-55 fluorescence spectrometer.

Transport experiments with vesicles isolated from Sf21 cells were described by Wlcek et al. (2013). In case of radioactive substrates, the filters were dissolved in Filter Count liquid scintillation cocktail from PerkinElmer. In case of experiments with fluorescent substrates, after the uptake the filters were incubated in 1 ml of 1% (w/v) Triton X-100 in an Eppendorf tube for 30 minutes and subsequently centrifuged for 40 minutes in an Eppendorf FA-45-30-11 rotor at 20,000g. The supernatant was used for fluorescence determination in a Perkin Elmer LS-55 fluorescence spectrometer.

Analytical Methods

The following settings were used for fluorescence measurements: for Dansyl (DNS) derivatives, excitation (ex) 335 nm (slit 20 nm) and emission (em) 520 nm (slit 20 nm); for 4-nitrobenzo[c][1,2,5]oxadiazole (NBD) derivatives, ex 478 nm (slit 20 nm) and em 545 nm (slit 20 nm); and for Pacific Blue (PB) derivatives, ex 410 nm (slit 5 nm) and em 451 nm (slit 5 nm). Standard curves were prepared with the fluorescent substrates in 1% (w/v) Triton X-100. A total membrane fraction of WT and ASBT-expressing cells was isolated as described by Huber et al. (2007) and used for Western blotting (Mahdi et al., 2016). Protein was quantified with the bicinchoninic acid method (Smith et al., 1985) using the BCA protein assay kit from Interchim (Montluçon, France).

Chemistry General Remarks

Reagents and solvents were purchased from commercial sources and were used without further purification or drying. Automated column chromatography was performed on a TeledyneISCO Combi-Flash Rf + machine on RediSepRf prepacked columns. Progress of chemical reactions was monitored on Alugram Xtra Sil G/UV254 TLC plates with detection of the compounds by UV-visible absorption at 254 nm and 366 nm. Compounds were analyzed by UPLC-MS, and their purity was assessed by analytical reversed-phase ultra performance liquid chromatography (RP-UPLC). RP-UPLC spectra were obtained from a Dionex Ultimate 3000 RSLC System and a Dionex Acclaim RSLC 120 column. The following elution method was used: A gradient from 100% A (milliQ deionized water with 0.05% trifluoroacetic acid) to 100% D (high-pressure liquid chromatography–grade acetonitrile/milliQ deionized water 9:1 with 0.05% trifluoroacetic acid) was applied for 4.5 minutes, and this was followed by 100% D washing. Low-resolution mass spectra were acquired on a Thermo Scientific LCQ Fleet by electron spray ionization in the positive mode. NMR spectra were recorded on a BRUKER Advance 300 (^{1}H at 300 MHz; ^{13}C at 75 MHz; ^{19}F at 282 MHz spectra) and a BRUKER Advance II 400 (^{1}H at 400 MHz and ^{13}C at 101 MHz spectra). Chemical shifts are given in parts per million (δ) referenced to TMS (δ = 0.00 ppm ^{1}H and ^{13}C NMR). The order of citation in parentheses is (1) multiplicity: s (singlet), d (doublet), t (triplet), q (quartet), m (multiplet), br (broad peak); (2) coupling constant (J) in Hz; and (3) number of equivalent nuclei (by integration). HSQC and HMBC were routinely used to assign peaks in ^{1}H and ^{13}C NMR spectra. High-resolution mass spectra (HRMS) measurements were performed by the Mass Spectrometry Service at the Department of Chemistry and Biochemistry, University of Bern, Switzerland on a Thermo Scientific LTQ OrbitrapXL. Absorption spectra were measured with a Varian Cary 100 Bio UV-visible spectrometer, and emission spectra were measured with a Varian Cary Eclipse fluorescence spectrometer. Copies of ^{1}H, ^{13}C, and ^{19}F NMR spectra of synthetic intermediates and final compounds and

UV-Vis absorption and fluorescence emission spectra of fluorescent probes are provided as Supplemental Data.

Compound Synthesis.

(2-Aminoethyl)cholic Amide. A solution of cholic acid (1 g, 2.45 mmol, 1 eq.) in methanol (25 ml) was treated with acetyl chloride (25 μl, 25 mg, 0.32 mmol, 0.13 eq.) at room temperature. The reaction was complete after 45 minutes. The solvent was concentrated in vacuo to give methyl cholate (1.1 g, quantitative) as a white foam (containing small amounts of MeOH). ^{1}H NMR (300 MHz, d_6-DMSO) δ 4.02 (br s, containing HDO, MeOH, and the three OH), 3.77 (s, 1H), 3.61 (d, J = 3.0, 1H), 3.57 (s, 3H), 3.27–3.09 (m, 1H, partially overlapped with the MeOH signal), 2.44–1.91 (m, 5H), 1.88–1.53 (m, 6H), 1.53–0.76 (m, 13H). 0.91 (d, J = 6.0, 3H), 0.80 (s, 3H), and 0.58 (s, 3H). HRMS m/z calculated for $C_{25}H_{42}N_5Na$ [M + Na]$^+$ 445.2924, which found 445.2917, Δ −1.70 ppm.

Methyl cholate (1.1 g, 2.62 mmol, 1 eq.) was added to ethylenediamine (5 ml, 74.79 mmol, 29 eq.), and the resulting solution was heated at reflux (140°C). After 3 hours the reaction was complete. The reaction solution was then cooled to room temperature, and ice water (50 ml) was added into the solution, after which a white precipitate formed. The solid was filtered, washed with cold water, and dried under reduced pressure to obtain (2-aminoethyl)cholic amide (**Cen**) (848 mg, 72%). ^{1}H NMR (300 MHz, d_6-DMSO) δ 7.69 (t, J = 5.6, 1H), 4.30 (s, 1H), 4.09 (s, 1H), 4.00 (d, J = 3.3, 1H), 3.78 (s, 1H), 3.61 (s, 1H), 3.18 (s, 1H), 3.00 (q, J = 6.2, 2H), 2.53 (q, J = 6.5, 2H), 2.32–0.74 (m, 26H), 0.92 (d, J = 6.2, 3H), 0.81 (s, 3H), and 0.58 (s, 3H). HRMS m/z was calculated for $C_{26}H_{47}N_2O_4$ [M + H]$^+$ 451.3530, which found 451.3517, Δ −2.98 ppm. LC-MS t_R 2.3 minutes, m/z [M + H]$^+$ 451.28.

(2-Aminoethyl)chenodeoxycholic Amide. Similarly to the synthesis of **Cen** above, chenodeoxycholic acid (1 g, 2.54 mmol, 1 eq.) was dissolved in MeOH (25 ml). Acetyl chloride (25 μl, 25 mg, 0.32 mmol, 0.13 eq.) was added at room temperature, and the resulting solution was stirred overnight. The solvent was concentrated in vacuo to give methyl chenodeoxycholate (1.1 g, quantitative) as a colorless oil. ^{1}H NMR (300 MHz, d_6-DMSO) δ 4.02 (br s, containing hydrodeoxygenation, MeOH, and the two OH), 3.77 (s, 1H), 3.62 (d, J = 2.8, 1H), 3.57 (s, 3H), 3.27–3.08 (m, 1H, partially overlapped with the MeOH signal), 2.42–2.08 (m, 3H), 1.97–1.53 (m, 7H), 1.53–0.78 (m, 16H), 0.88 (d, J = 6.4, 3H), 0.83 (s, 3H), 0.60 (s, 3H). HRMS m/z was calculated for $C_{25}H_{42}NaO_4$ [M + Na]$^+$ 429.2975, which found 429.2964, Δ −2.66 ppm.

Methyl chenodeoxycholate (1.1 g, 2.68 mmol, 1 eq.) was added to ethylenediamine (5 ml, 74.79 mmol, 28 eq.). The resulting solution was stirred overnight at room temperature and refluxed (140°C) for 2 hours. After that time, the reaction was complete. The reaction solution was then cooled to room temperature, and ice water (7 ml) was added into the solution at -10°C. A white precipitate formed. The solid was filtered, washed with cold water, and dried under reduced pressure. ^{1}H NMR analysis of the solid showed presence of ethylenediamine, which was responsible for the formation of an undesired byproduct in the next step. The solid was repurified chromatographically (Combi-Flash, SiO$_2$, 100% EtOAc) to obtain (2-aminoethyl)chenodeoxycholic amide (**CDCen**) (720 mg, 62%). ^{1}H NMR (300 MHz, d_6-DMSO) δ 7.70 (t, J = 5.6, 1H), 4.31 (d, J = 4.6, 1H), 4.11 (d, J = 3.4, 1H), 3.62 (s, 1H), 3.17 (s, 1H), 3.00 (q, J = 6.2, 2H), 2.53 (q, J = 6.7, 2H), 2.34–1.54 (m, 10H), 1.53–0.85 (m, 18 H), 0.88 (d, J = 6.5, 3H), 0.83 (s, 3H), and 0.60 (s, 3H). HRMS m/z was calculated for $C_{26}H_{47}N_2O_3$ [M + H]$^+$ 435.3581, which found 435.3582, Δ 0.25 ppm. LC-MS t_R 2.97 minutes, m/z [M + H]$^+$ 435.38.

CenNBD. 4-Chloro-7-nitrobenzofurazan (60 mg, 0.3 mmol, 1.5 eq.) was dissolved in anhydrous N,N-dimethylformamide (DMF) (2 ml). After the addition of triethylamine (60 μl, 44 mg, 0.44 mmol, 2.2 eq.) and **Cen** (90 mg, 0.2 mmol, 1 eq.), the mixture was stirred at room temperature for 3 hours. The reaction solution was diluted with water (30 ml) and extracted with ethyl acetate (5 × 15 ml). The organic layer was washed with water (5 × 10 ml) and then dried over Na$_2$SO$_4$.

After evaporation under reduced pressure, a brown-green solid was obtained. The crude was purified by CombiFlash (SiO$_2$, 4 g, EtOAc/MeOH 10:0 to 8:2, compounds eluted between 15% and 20% MeOH). The final compound was isolated as a yellow/reddish solid (58 mg, 48%). ^{1}H NMR (300 MHz, d_6-DMSO) δ 9.40 (s, 1H), 8.53 (d, J = 8.9, 1H), 8.00 (t, J = 5.8, 1H), 6.43 (d, J = 9.0, 1H), 4.30 (d, J = 4.2, 1H), 4.07 (d, J = 3.3, 1H), 3.99 (d, J = 3.4, 1H), 3.72 (d, J = 3.3, 1H), 3.56 (m, 3H), 3.39 (q, J = 5.7, 1H), 3.17 (m, 1H), 2.30–1.86 (m, 6H), 1.86–1.50 (m, 6H), 1.50–0.69 (m, 16H), 0.87 (d, J = 6.1, 3H), 0.79 (s, 3H), and 0.49 (s, 3H). ^{13}C NMR (75 MHz, d_6-DMSO) δ 173.40, 145.36, 144.39, 144.06, 137.85, 120.82, 99.11, 70.94, 70.40, 66.20, 48.56, 46.04, 45.65, 43.26, 41.49, 41.27, 39.44, 35.27, 34.95, 34.86, 34.34, 32.42, 31.46, 30.37, 28.50, 27.18, 26.31, 26.17, 22.70, 22.55, 17.06, and 12.22. HRMS m/z was calculated for C$_{32}$H$_{48}$N$_5$O$_7$ [M + H]$^+$ 614.3548, which found 614.3554, Δ 0.97 ppm. LC-MS t_R 3.57 minutes, 99% pure (at λ_{214nm}). UV-visible/Fluo (PBS buffer + 1% DMSO): $\lambda_{max\ abs}$ 478 nm, $\lambda_{max\ em}$ 545 nm.

CDCenNBD. Analogously to **CenNBD**, the title compound was prepared from 4-chloro-7-nitrobenzofurazan (60 mg, 0.3 mmol, 1.5 eq.) and **CDCen** (86 mg, 0.2 mmol, 1 eq.) in the presence of triethylamine (60 μl, 44 mg, 0.44 mmol, 2.2 eq.) in DMF (2 ml). The crude was purified twice by CombiFlash (SiO$_2$, 4 g, EtOAc/MeOH 10:0 to 8:2) to obtain the final compound as a yellow/reddish solid (50 mg, 42%). ^{1}H NMR (300 MHz, d_6-DMSO) δ 9.40 (s, 1H), 8.53 (d, J = 8.9, 1H), 8.01 (t, J = 5.7, 1H), 6.43 (d, J = 9.0, 1H), 4.30 (d, J = 4.6, 1H), 4.09 (d, J = 3.4, 1H), 3.56 (m, 3H), 3.38 (q, J = 5.8, 2H), 3.25–3.10 (m, 1H), 2.33–1.52 (m, 12H), 1.52–0.72 (m, 24H), and 0.51 (s, 3H). ^{13}C NMR (101 MHz, d_4-MeOD) δ 177.71, 146.83, 145.80, 145.39, 138.47, 123.30, 99.95, 72.84, 69.03, 57.20, 51.42, 44.68, 43.59, 43.11, 40.90, 40.70, 40.41, 39.08, 36.71, 36.51, 36.16, 35.83, 34.07, 33.97, 33.12, 31.32, 29.17, 24.53, 23.36, 21.70, 18.89, and 12.12. HRMS m/z was calculated for C$_{32}$H$_{48}$N$_5$O$_6$ [M + H]$^+$ 598.3599, which found 598.3592, Δ −1.24 ppm. LC-MS t_R 3.86 minutes, 95% pure (at λ_{214nm}).

AcenNBD. The same procedure was used as for **CenNBD** above. 4-Chloro-7-nitrobenzofurazan (293 mg, 1.47 mmol, 1.47 eq.) and N-(2-aminoethyl) acetamide (95 μl, 102 mg, 1 mmol, 1 eq.) reacted in the presence of triethylamine (300 μl, 218 mg, 2.15 mmol, 2.2 eq.) in DMF (10 ml). The crude was purified by CombiFlash (SiO$_2$, 12 g, EtOAc/MeOH 10:0 to 8:2). Only the purest fractions were collected, as many were contaminated with traces of a fluorescent byproduct, and the final compound was isolated as a yellow/reddish solid (22 mg, 8%). ^{1}H NMR (300 MHz, d_6-DMSO) δ 9.44 (br s, 1H), 8.54 (d, J = 8.9, 1H), 8.07 (t, J = 5.9, 1H), 6.43 (d, J = 9.0, 1H), 3.53 (br s, 2H), 3.35 (q, J = 6.1, 2H), and 1.80 (s, 3H). ^{13}C NMR (101 MHz, d_6-DMSO) δ 169.94, 145.37, 144.46, 144.10, 137.93, 120.86, 99.12, 43.10, 37.28, and 22.58. HRMS m/z was calculated for C$_{10}$H$_{11}$N$_5$O$_4$ [M + H]$^+$ 266.0884, which found 266.0884, Δ 0.04 ppm. LC-MS t_R 2.02 minutes, >90% pure (at λ_{214nm}).

CenDNS. Dansyl chloride (30 mg, 0.11 mmol, 1.1 eq.) was dissolved in dichloromethane (DCM) (1 ml) and added to **Cen** (45 mg, 0.1 mmol, 1 eq.) in DCM (1 ml) at 0°C, which was followed by the addition of triethylamine (30 μl, 22 mg, 0.22 mmol, 2.2 eq.). The resulting solution was stirred overnight while slowly warming up to room temperature. After 18 hours, the reaction solution was diluted with aq. NaHCO$_3$ (5 ml) and extracted with ethyl acetate (3 × 25 ml), and the organic layer was dried over Na$_2$SO$_4$ and evaporated under reduced pressure. The crude was purified by CombiFlash (SiO$_2$, 12 g, EtOAc/MeOH 10:0 to 8:2). The title compound was obtained as pale yellow solid (51 mg, 75%). ^{1}H NMR (300 MHz, d_6-DMSO) δ 8.46 (dt, J = 8.5, 1.1, 1H), 8.26 (d, J = 8.6, 1H), 8.08 (dd, J = 7.3, 1.2, 1H), 7.94 (t, J = 5.8, 1H), 7.69 (t, J = 5.7, 1H), 7.60 (m, 2H), 7.26 (dd, J = 7.7, 0.9, 1H), 4.31 (d, J = 4.3, 1H), 4.07 (d, J = 3.6, 1H), 3.99 (d, J = 3.4, 1H), 3.75 (d, J = 3.4, 1H), 3.60 (br s, 1H), 3.25–3.10 (m, 1H), 3.02 (q, J = 6.3, 2H), 2.83 (s, 6H), 2.76 (q, J = 6.2, 2H), 2.37–0.76 (m, 24H), 0.87 (d, J = 6.2, 3H), 0.81 (s, 3H), and 0.53 (s, 3H). ^{13}C NMR (101 MHz, d_4-MeOD) δ 177.16, 153.29, 136.74, 131.29 (2C), 130.92, 130.29, 129.21, 124.31, 120.45, 116.47, 74.04, 72.89, 69.05, 48.00, 47.48, 45.81 (2C N(CH$_3$)$_2$), 43.34, 43.22, 43.00, 41.03, 40.49, 40.28, 36.83, 36.50, 35.91, 33.98, 33.07, 31.20, 30.73, 29.60, 28.66, 27.89, 24.21, 23.17, 17.74, and 12.99. ^{13}C NMR (101 MHz, d_6-DMSO) δ 172.76, 151.35, 135.73, 129.42, 129.05,

128.98, 128.26, 127.83, 123.52, 118.97, 115.11, 70.95, 70.39, 66.20, 48.55, 46.03, 45.67, 45.03, 41.95, 41.49, 41.32, 38.46, 35.28, 35.01, 34.86, 34.35, 32.37, 31.47, 30.37, 28.52, 27.22, 26.18, 22.73, 22.59, 17.05, and 12.26 (one signal overlapped with the solvent signal). HRMS m/z was calculated for C$_{38}$H$_{58}$N$_3$O$_6$S [M + H]$^+$ 684.4041, which found 684.4043, Δ 0.32 ppm. LC-MS t_R 3.48 minutes, 97% pure (at λ_{214nm}). UV-visible/Fluo (MeOH + 1% DMSO): $\lambda_{max\ abs}$ 334 nm, $\lambda_{max\ em}$ 520 nm.

CDCenDNS. The procedure above was used for the synthesis of **CDCenDNS**, starting from dansyl chloride (60 mg, 0.22 mmol, 1.1 eq.) and **CDCen** (86 mg, 0.2 mmol, 1 eq.) in DCM (2 ml) and triethylamine (60 μl, 44 mg, 0.44 mmol, 2.2 eq.). After purification by CombiFlash (SiO$_2$, 4 g, EtOAc/MeOH 10:0 to 8:2), the final compound was isolated as a pale yellow solid (81 mg, 61%). ^{1}H NMR (300 MHz, d_6-DMSO) δ 8.46 (d, J = 8.5, 1H), 8.26 (d, J = 8.7, 1H), 8.08 (dd, J = 7.3, 1.3, 1H), 7.94 (t, J = 5.9, 1H), 7.69 (t, J = 5.7, 1H), 7.60 (m, 2H), 7.26 (d, J = 7.4, 1H), 4.31 (d, J = 4.7, 1H), 4.10 (d, J = 3.5, 1H), 3.62 (s, 1H), 3.02 (q, J = 6.5, 2H), 2.83 (s, 6H), 2.76 (q, J = 6.6, 2H), 2.19 (q, J = 12.9, 1H), 2.07–0.66 (m, 35H), and 0.54 (s, 3H). ^{13}C NMR (75 MHz, d_4-MeOD) δ 177.07, 153.17, 136.67, 131.25, 131.17, 130.86, 130.25, 129.19, 124.29, 120.40, 116.37, 72.80, 68.96, 57.15, 51.46, 45.82, 43.60, 43.32, 43.10, 40.98, 40.70, 40.41, 40.37, 36.77, 36.53, 36.17, 35.87, 33.98, 33.94, 33.04, 31.34, 29.21, 24.58, 23.43, 21.75, 18.94, and 12.22. HRMS m/z was calculated for C$_{38}$H$_{58}$N$_3$O$_5$S [M + H]$^+$ 668.4092, which found 668.4080, Δ −1.72 ppm. LC-MS t_R 3.80 minutes, 99% pure (at λ_{214nm}).

AcenDNS. This control compound was prepared similarly to **CenDNS** and **CDCenDNS** from N-(2-aminoethyl) acetamide (95 μl, 102 mg, 1 mmol, 1 eq.) and dansyl chloride (290 mg, 1.077 mmol, 1.077 eq.) in DCM (7.5 ml) and triethylamine (300 μl, 218 mg, 2.15 mmol, 2.2 eq.). The crude was purified by CombiFlash (SiO$_2$, 12 g, EtOAc/MeOH 10:0 to 8:2) to obtain **AcenDNS** as a pale yellow solid (275 mg, 82%). ^{1}H NMR (300 MHz, d_6-DMSO) δ 8.47 (d, J = 8.5, 1H), 8.28 (d, J = 8.7, 1H), 8.10 (dd, J = 7.3, 1.2, 1H), 7.96 (br s, 1H), 7.77 (t, J = 5.6, 1H), 7.63 (dd, J = 8.6, 7.3, 1H), 7.60 (dd, J = 8.5, 7.7, 1H), 7.27 (dd, J = 7.6, 0.9, 1H), 3.09–2.93 [m (pseudo q), 2H], 2.84 (s, 6H), 2.79 (t, J = 6.9, 2H), and 1.69 (s, 3H). ^{13}C NMR (101 MHz, d_6-DMSO) δ 169.32, 151.37, 135.75, 129.45, 129.07, 129.00, 128.30, 127.86, 123.58, 119.03, 115.14, 45.06, 41.91, 38.62, and 22.45. HRMS m/z was calculated for C$_{16}$H$_{21}$N$_3$O$_3$S [M + H]$^+$ 336.1376, which found 336.1370, Δ −1.90 ppm. LC-MS t_R 2.32 minutes, >90% pure (at λ_{214nm}).

CenPB. Amine **Cen** (13 mg, 0.029 mmol, 1 eq.) was dissolved in DMF (0.8 ml). Diisopropylethylamine (100 μl, 76 mg, 0.59 mmol, 20 eq.) was added, which was followed by Pacific Blue succinimidyl ester (10 mg, 0.029 mmol, 1 eq.). The mixture was stirred for 3 hours at room temperature, after which the reaction mixture was evaporated under reduced pressure. The crude was purified by column chromatography (SiO$_2$, EtOAc/MeOH 8:2), and the obtained compound was recrystallized from water/MeOH (4:1). The pale yellow solid was filtered, washed with cold water, and dried in vacuo to yield **CenPB** (11 mg, 55%). ^{1}H NMR (300 MHz, d_6-DMSO) δ 11.95 (br s, 1H) 8.63 (m, 2H), 7.86 (t, J = 5.3, 1H), 7.51 (d, J = 10.9, 1H), 4.29 (br s, 1H), 4.06 (m, 2H), 3.97 (br s, 1H), 3.72 (d, J = 3.4, 1H), 3.56 (br s, 1H), 3.4–3.11 (m, 4H, partially overlapped with the solvent signal), 2.34–1.85 (m, 6H), 1.86–1.53 (m, 6H), 1.48–1.02 (m, 10H), 1.02–0.73 (m, 2H), 0.89 (d, J = 6.2, 3H), 0.77 (s, 3H), and 0.48 (s, 3H). ^{13}C NMR (101 MHz, d_6-DMSO) δ 173.34, 162.68, 160.82, 147.69, 110.30 (d, J = 22.5), 71.48, 70.93, 66.71, 49.07, 46.71, 46.18, 42.02, 41.75, 39.28, 38.77, 35.78, 35.43, 35.34, 34.84, 33.06, 32.09, 30.88, 28.96, 27.72, 26.65, 23.23, 23.01, 17.57, 12.72. ^{19}F NMR (282 MHz, d_6-DMSO) δ −135.66 (br s). HRMS m/z was calculated for C$_{36}$H$_{49}$F$_2$N$_2$O$_8$ [M + H]$^+$ 675.3451, which found 675.3453, Δ 0.24 ppm. LC-MS t_R 3.23 minutes, 97% pure (at λ_{214nm}). UV-visible/Fluo (PBS buffer + 1% DMSO): $\lambda_{max\ abs}$ 410 nm, $\lambda_{max\ em}$ 451 nm.

CDCenPB. Analogously to above, **CDCen** (50 mg, 0.115 mmol, 1 eq.) was dissolved in DMF (2 ml). Diisopropylethylamine (200 μl, 152 mg, 1.176 mmol, 10 eq.) was added, which was followed by Pacific Blue succinimidyl ester (39 mg, 0.115 mmol, 1 eq.). The mixture was stirred for 4 hours at room temperature, and the reaction mixture was

evaporated under reduced pressure. The crude was purified by CombiFlash (SiO₂, 4 g, EtOAc/MeOH 10:0 to 8:2) to give **CDCenPB** (38 mg, 50%). ¹H NMR (300 MHz, d_6-DMSO) δ 8.69 (d, J = 1.6, 1H), 8.64 (t, J = 5.7, 1H), 7.87 (t, J = 5.4, 1H), 7.59 (d, J = 10.7, 1H), 4.29 (br s, 1H), 4.13–4.01 (m, 2H), 3.57 (br s, 1H), 3.44–3.10 (m, 4H, partially overlapped with the solvent signal), 2.33–0.85 (m, 26H), 0.85 (d, J = 6.3, 3H), 0.80 (s, 3H), and 0.49 (s, 3H). ¹³C NMR (101 MHz, d_4-MeOD) δ 177.17, 164.63, 162.00, 152.24 (d, J = 243.0), 149.23, 147.00, 142.68 (dd, J = 38.0, 7.9), 140.06 (d, J = 6.5), 114.30, 110.89 (d, J = 21.3), 109.17–108.68 (m), 72.86, 69.01, 57.40, 51.43, 43.61, 43.16, 40.96, 40.74, 40.45, 40.29, 39.88, 36.72, 36.53, 36.17, 35.87, 34.21, 33.96, 33.21, 31.33, 29.21, 24.57, 23.33, 21.71, 18.91, and 12.17. ¹⁹F NMR (282 MHz, d_6-DMSO) δ -135.48 (br s). HRMS m/z was calculated for C₃₆H₄₈F₂N₂NaO₇ [M + Na]⁺ 681.3322, which found 681.3309, Δ −1.86 ppm. LC-MS t_R 3.53 minutes, 98% pure (at λ_{214nm}).

AcenPB. As above, N-(2-aminoethyl) acetamide (20 μl, 21 mg, 0.209 mmol, 1.77 eq.) and Pacific Blue succinimidyl ester (40 mg, 0.118 mmol, 1 eq.) reacted in the presence of diisopropylethylamine (100 μl, 76 mg, 0.59 mmol, 20 eq.) in DMF. The crude was purified by CombiFlash (SiO₂, 4 g, EtOAc/MeOH 10:0 to 8:2) to obtain **AcenPB** as a pale yellow solid (25 mg, 68%). ¹H NMR (300 MHz, d_6-DMSO) δ 12.10 (s, 1H), 8.70 (d, J = 1.6, 1H), 8.66 (t, J = 5.8, 1H), 7.96 (t, J = 5.5, 1H), 7.61 (d, J = 11.1, 1H), 3.36 (q, J = 6.1, 2H), 3.19 (q, J = 6.1, 2H), and 1.80 (s, 3H). ¹³C NMR (101 MHz, d_6-DMSO) δ 169.49, 161.97, 160.12, 150.40 (dd, J = 240.9, 5.5), 147.27 (t, J = 3.3), 146.29–145.41 (m), 141.28 (d, J = 8.4), 139.56 (dd, J = 242.1, 7.9), 112.06, 110.06 (dd, J = 21.1, 3.0), 106.66–105.90 (m), 38.86, 38.36, and 22.60. ¹⁹F NMR (282 MHz, d_6-DMSO) δ −135.47 (t, J = 11.3). HRMS m/z was calculated for C₁₄H₁₂F₂N₂O₅ [M + H]⁺ 327.0787, which found 327.0789, Δ 0.72 ppm. LC-MS t_R 1.94 minutes, >90% pure (at λ_{214nm}).

Results

Synthesis of Fluorescent Bile Salt Probes. Previous examples of fluorescent BS derivatives indicate that the carboxylic acid side chain at C-24 of the bile acid skeleton is tolerant toward substitution with fluorescent dyes and other moieties (Holzinger et al., 1997; Yamaguchi et al., 2006; Rais et al., 2010; Dong et al., 2015; Testa et al., 2017). In addition, we have decided to introduce a short ethylene diamine linker

unit to mimic the amino acids glycine and taurine, which are commonly conjugated at this position in human bile acids (Fig. 1A). With regards to the choice of fluorescent dyes, we reasoned that small organic fluorescent dyes would interfere the least with the transport mechanisms, and therefore we conjugated NBD, DNS, and PB to the C-24 position of cholic and chenodeoxycholic acid (Fig. 1B). Furthermore, these three dyes could potentially mimic certain features of the natural transport substrates; NBD and DNS both have slightly acidic NH groups, the sulfonamide group of DNS is similar to the sulfonic acid end group of taurine, and, due to the two strongly electron-withdrawing fluorine atoms, the phenol group of PB is always deprotonated under physiologic conditions like the end groups of human bile acids (Fig. 1A).

The synthesis of the fluorescent BS derivatives started from cholic or chenodeoxycholic acid, which were transformed to the corresponding methyl esters (Scheme 1A). Aminolysis in refluxing ethylenediamine yielded the two amide building blocks **Cen** and **CDCen**. It is important at this point to quantitatively remove any remaining ethylenediamine. The three fluorescent dyes were then coupled to the primary amine terminus of **Cen** and **CDCen** using standard conditions and commercial dye reagents NBD chloride, dansyl chloride, and Pacific Blue N-hydroxysuccinimid ester. The isolated final probes were subjected to a number of purification steps, including washing, precipitation, and chromatographic methods, to ensure that all traces of uncoupled fluorescent dyes were removed. This is crucial, as several studies in the past have shown that fluorescent dyes alone can also act as transport substrates (De Bruyn et al., 2011; Patik et al., 2015, 2018). Consequently, our extensive purification efforts delivered the final fluorescent BS probes in high purity (>95% according to NMR and high-pressure liquid chromatography) albeit at the expense of isolated yields (42–75%). In a similar fashion, we have also generated truncated control compounds **AcenNBD**, **AcenDNS**, and **AcenPB**, which lack the bile acid moiety. All final compounds showed strong fluorescence emission in the region of 450–550 nm (Scheme 1B).
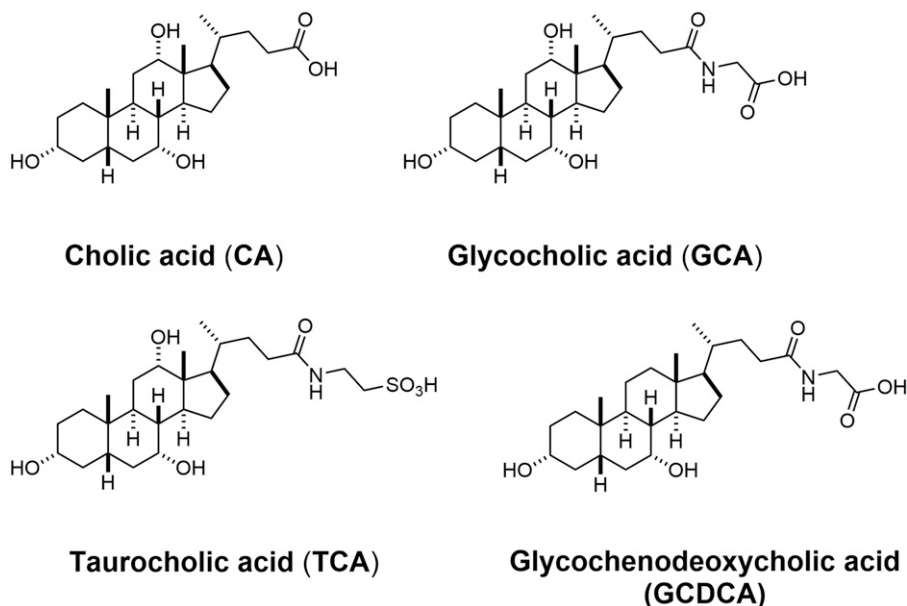

Cholic acid (CA)

Glycocholic acid (GCA)

Taurocholic acid (TCA)

Glycochenodeoxycholic acid (GCDCA)

Fig. 1. (A) Structures of common human bile salts. (B) Structures of synthetic fluorescent bile salt derivatives.
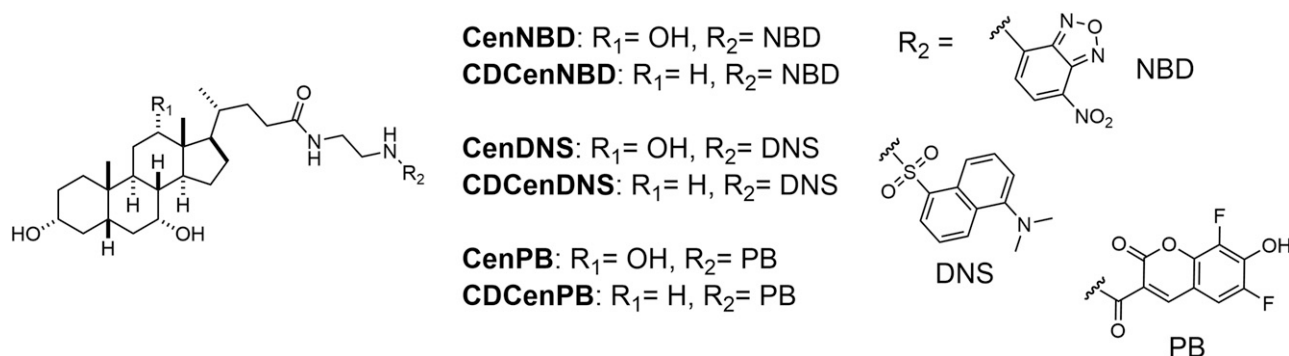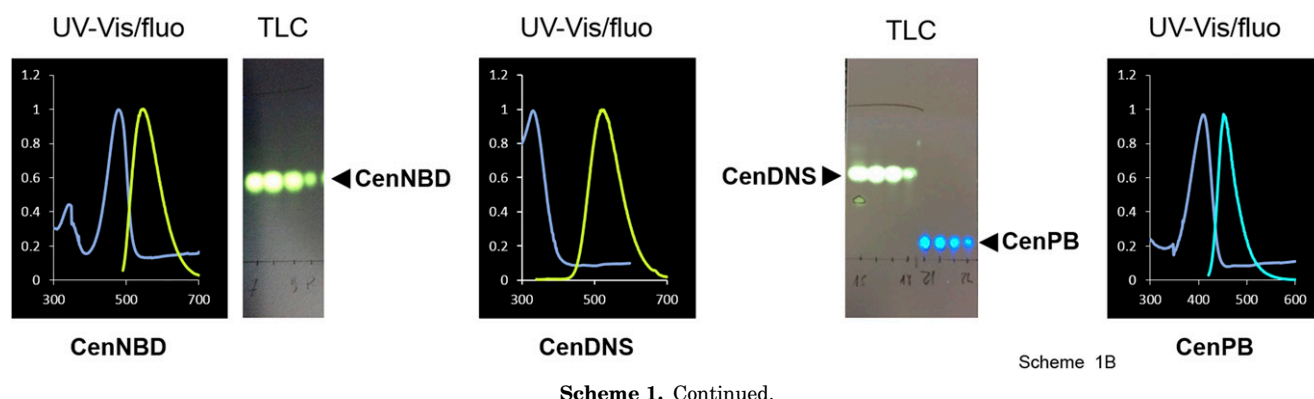
Fig. 1. Continued.

Generation of CHO-ASBT Cells. To demonstrate the successful transfection of CHO cells with functional ASBT, we determined their capacity for sodium-dependent BS uptake. Figure 2A shows sodium-dependent uptake into transfected CHO cells, which is absent in wild-type CHO cells. Figure 2B confirms expression of ASBT by Western blotting and expression at the plasma membrane of transfected CHO cells by immunofluorescence, which is again absent in wild-type cells. Hence, we successfully established an ASBT-expressing CHO cell line. For a final characterization of this novel cell line, we

determined the concentration dependence of sodium-dependent uptake of taurocholate under initial uptake conditions. Figure 3 shows that the K_m value is about 34 μM, which is in line with published values (Craddock et al., 1998).

Inhibition of Transporters by Fluorescent Bile Salt Probes. To test the different fluorescent BS derivatives as potential substrates of BS and organic anion transporters, we chose a two-tier approach. First, the new BS derivatives were tested as potential inhibitors of a radioactively labeled standard substrate for the respective carrier. Derivatives
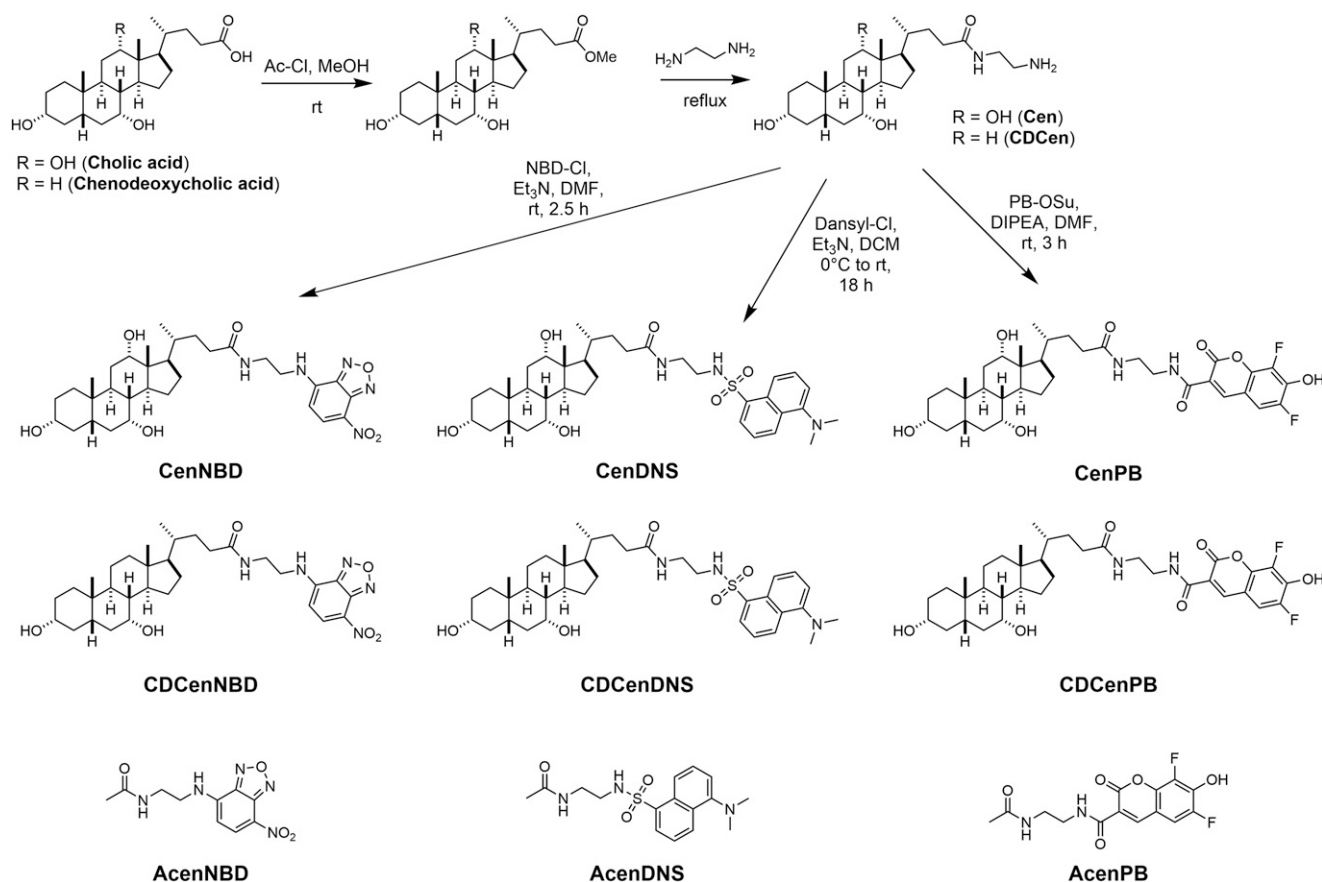
Scheme 1. (A) Chemical synthesis of fluorescent bile salt derivatives. Reagents: Ac-Cl, acetyl chloride; Et$_3$N, triethylamine; DMF; DCM; PB-OSu, PB N-hydroxysuccinimid ester; DIPEA, N,N-diisopropylethylamine. (B) Absorption and emission properties of fluorescent bile salt derivatives. Normalized UV-visible absorption and fluorescence emission spectra, **CenNBD**: λ_{max} abs 478 nm, λ_{max} em 545 nm; **CenDNS**: λ_{max} abs 334 nm, λ_{max} em 520 nm; **CenPB**: λ_{max} abs 410 nm, λ_{max} em 451 nm. TLC, spotted compounds run on thin-layer chromatography plates (silica gel; ethyl acetate/methanol 8:2) and excited at 366 nm. Note the difference in polarity between **CenDNS** and **CenPB**.

Scheme 1. Continued.

inhibiting transport were secondly tested as potential substrates by performing a transport experiment. Table 1 lists the uptake of standard substrates for all transporters investigated. Comparing transport under control and transporter-mediated conditions shows for all transporters a transporter-to-control ratio of more than 2.5, which makes the test systems amenable for the inhibition studies. Figure 4 shows a typical inhibition experiment with an uptake transporter. This figure clearly demonstrates the concentration-dependent inhibition of OATP1B1-mediated estrone-3-sulfate by **CenNBD**. It should also be noted, that **CenNBD** did not affect the plasma membrane barrier function of the cells, as even at 100 µM no increase of estrone-3-sulfate uptake into WT cells was found. Figure 5 gives an example of the efflux transporter BSEP. Here, ATP-dependent uptake of taurocholate was inhibited by **CDCenNBD** in a concentration-dependent manner. Similarly, no impact on vesicle membrane barrier function was found, as evidenced by an unchanged taurocholate transport in the absence of ATP. Because of the number of compounds to be tested on a large number of transporters, the experiments were not designed to obtain IC_{50} values for inhibiting fluorescent BS derivatives. Table 2 shows the summary of the inhibition experiments with uptake transporters. The pattern of inhibition is somewhat unexpected, as NTCP is strongly inhibited in a concentration-dependent manner by all fluorescent BS derivatives with the exception of **CDCenDNS**, which inhibits up to ~55% at 100 µM. This

finding contrasts to some extent with the known restricted substrate specificity of NCTP (Stieger, 2011). Among the OATPs, the pattern is different and transporter-specific: Strong inhibition was observed for **CenNBD** against OATP1B3 and OATP2B1; **CenDNS** against OATP1B1 and OATP2B1; **CenPB** against OATP1B3; and **CDCenPB** against OATP1B1, OATP1B3, and OATP2B1. A weaker inhibition was found for **CenNBD** against OATP1B1, **CenDNS** against OATP1B3, **CenPB** against OATP1B1 and OATP2B1, **CDCenNBD** against OATP1B3 and OATP2B1, and **CDCenDNS** against OATP1B3 and OATP2B1. No relevant inhibition was observed for **CDCenNBD** against OATP1B1 and **CDCenDNS** against OATP1B1. Given the known broad substrate specificity of OATPs (Obaidat et al., 2012; Hagenbuch and Stieger, 2013), a good inhibition of most OATPs was anticipated. Finally, we also tested the intestinal BS transporter ASBT. Unexpectedly, not one of the derivatives was a strong inhibitor: With the exception of **CDCenDNS** and **CDCenNBD** (no
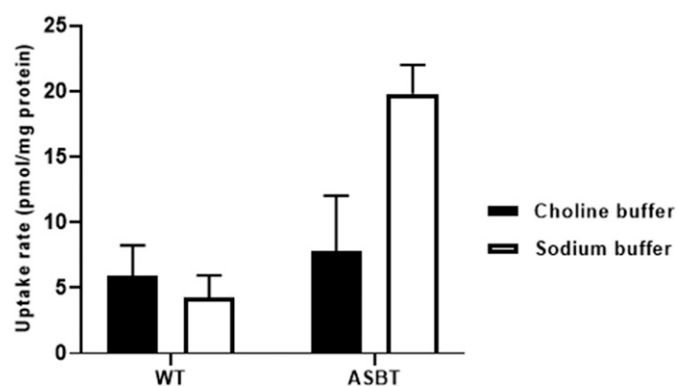
Fig. 2. Characterization of ASBT-expressing CHO cells. (A) Uptake of 5 µM taurocholate in WT and ASBT-expressing cells was measured for 3 minutes in the presence or absence of sodium as described in *Materials and Methods*. (B) Left: Western blot of WT and ASBT-expressing cells. The band for ASBT is indicated by an arrow. Right: immunolocalization of ASBT at the plasma membrane of transfected cells (upper panel).
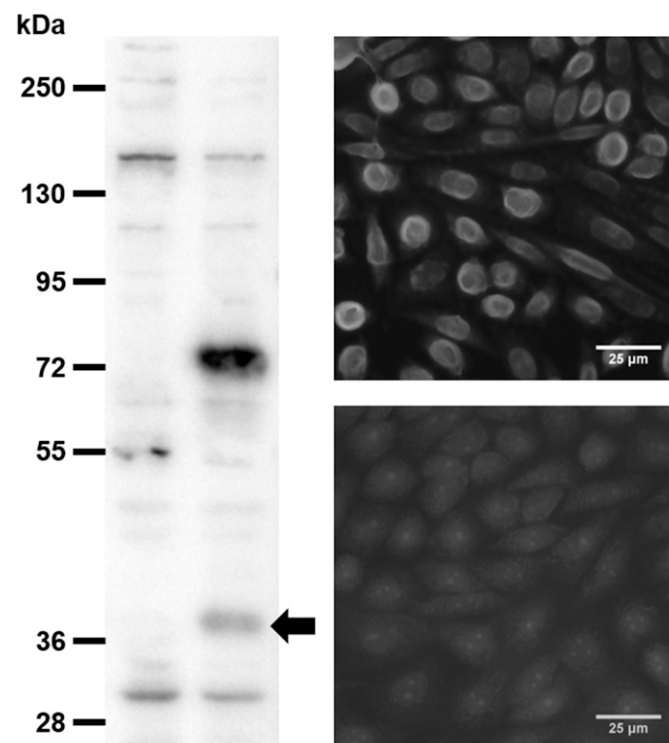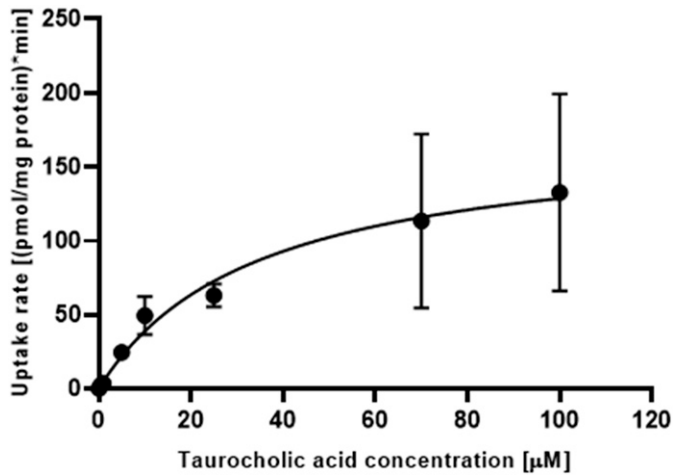

Fig. 2. Continued.

Fig. 3. Kinetic analysis of taurocholate transport into ASBT-CHO cells. Taurocholate uptake was determined as described in *Materials and Methods* over 1 minute. Uptake was calculated as difference between uptake in the presence of sodium and in the presence of choline. Data are mean ± S.D. of an experiment with triplicates.

inhibition), all derivatives were weak inhibitors. To exclude an interference of the fluorophores with the transporter, truncated probes **AcenNBD**, **AcenDNS**, and **AcenPB** were also tested but showed no relevant interaction with transport of test substrates (Table 2). The efflux transporter BSEP was strongly inhibited by all BS derivatives, whereas the unconjugated fluorophores showed no interaction (Table 3). In contrast, MRP2 tended to be stimulated rather than inhibited by the NBD and DNS conjugates of the bile acids (Table 3). However, this stimulation was also observed by the respective unconjugated fluorophores **AcenNBD** and **AcenDNS**. In contrast, **AcenPB** showed no interaction with MRP2, whereas **CDCenPB** stimulated MRP2 transport activity at 10 μM but acted as an inhibitor at 100 μM. The unconjugated **AcenPB** did not inhibit MRP2-mediated transport of estradiol 17β-D-glucuronide.

Transport of Fluorescent Bile Salt Probes. Finally, we assessed the fluorescent BS derivatives, which were positive in the inhibition assay as potential transport substrates of the investigated organic anion transporters. The data for the uptake transporters are presented in Table 4. Overall, most inhibitory interactions did not result in positive transport data. None of the truncated fluorescent probes turned out to be a substrate of any transporter investigated. As the **CenPB**
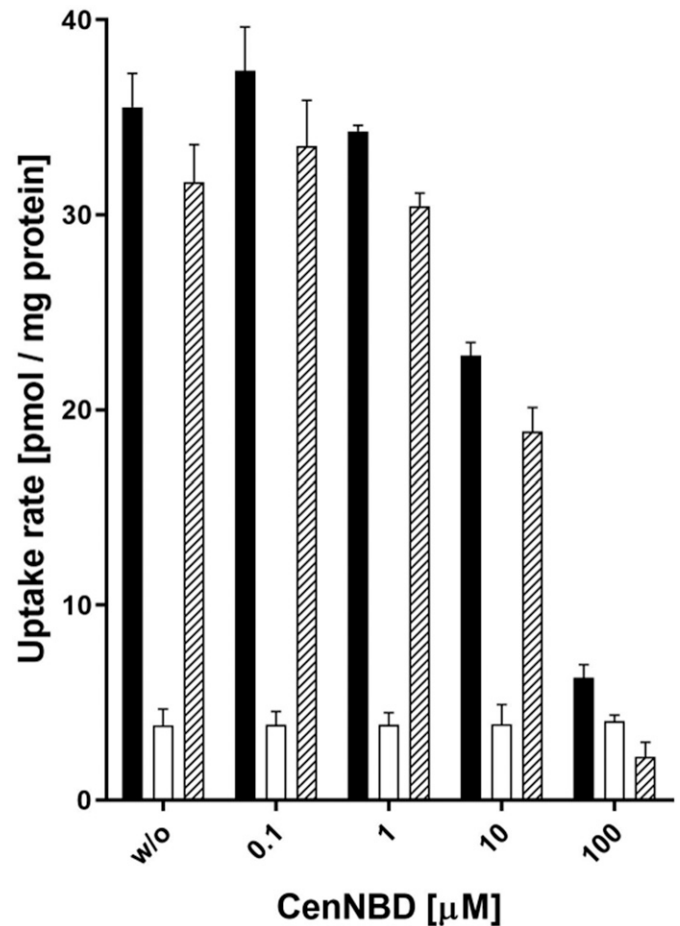

Fig. 4. Inhibition of 1 μM taurocholate uptake into WT (open bars) and OATP1B1 CHO cells (closed bars) in the presence of increasing concentrations **CenNBD**. The difference between OATP1B1 CHO and WT cells (hatched bars) is taken as OATP1B1-mediated transport. Transport was determined for 40 seconds as described in *Materials and Methods*. Data are mean ± S.D. of a representative experiment with three technical replicates.

derivatives were neither a substrate for NTCP nor for ASBT, **AcenPB** was not tested on these two transporters (Table 4). ASBT does not transport any of the tested fluorescent BS derivatives, and NTCP accepts **CenDNS** as substrate at low capacity. **CenNBD** is a low-capacity substrate of OATP1B1 and OATP2B1. **CenDNS** is well transported by OATP1B3 and

TABLE 1

Uptake rates of tested transport systems

Transport experiments were performed as described in *Material and Methods* using the substrates and conc. given in the table. Uptake was normalized to picomole per milligram protein × minute. The ratio was calculated by dividing transporter-mediated uptake rates by uptake rates under control conditions. Data are given as mean ± S.D.

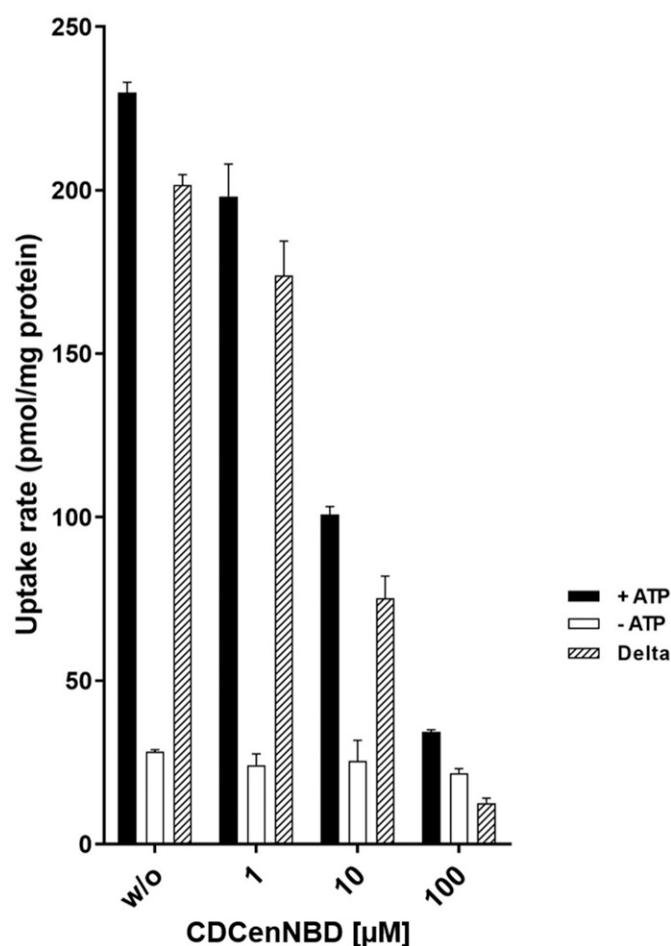| Transport System	Substrate	Conditions		Ratio	n
		Choline Buffer	Sodium Buffer		
NTCP	5 μM taurocholate	39.6 ± 20.9	135 ± 77	3.6 ± 1.7	12
ASBT	1 μM taurocholate	9.07 ± 3.89	44.9 ± 13.7	5.0 ± 2.8	8
		WT	Transfected		
OATP1B1	1 μM estrone-3-sulfate	6.62 ± 2.06	78.8 ± 30.5	12.7 ± 0.9	15
OATP1B3	5 μM taurocholate	19.0 ± 6.9	69.9 ± 18.9	3.9 ± 1.1	12
OATP2B1	1 μM estrone-3-sulfate	6.77 ± 2.20	69.1 ± 23.6	11.4 ± 5.3	13
		Without ATP	With ATP		
BSEP	2 μM taurocholate	6.97 ± 1.77	39.9 ± 10.8	6.2 ± 2.8	11
MRP2	10 μM estradiol 17β-D-glucuronide	24.9 ± 3.2	61.7 ± 8.3	2.5 ± 0.4	8

Fig. 5. Inhibition of 2 µM taurocholate uptake in the absence (open bars) and presence of ATP (closed bars) into BSEP-expressing insect cell vesicles cells in the presence of increasing concentrations **CDCenNBD**. The difference between uptake in the presence and absence of ATP (hatched bars) is taken as BSEP-mediated transport. Transport was determined for 5 minutes as described in *Materials and Methods*. Data are mean ± S.D. of a representative experiment with three technical replicates.

OATP2B1. Similar to **CenNBD**, **CenPB** is a low-capacity substrate of OATP1B1, but it is also a substrate of OATP1B3. **CDCenNBD** turned out to be a substrate for all hepatocellular OATPs, whereas **CDCenDNS** and **CDCenPB** are only transported by OATP1B3 and OATP2B1. Table 5 demonstrates that the ATP-binding cassette (ABC) transporters BSEP and MRP2 do not transport the new fluorescent bile acid derivatives. **CenPB** (BSEP) and **CDCenPB** (BSEP and MRP2) were both positive in two independent experiments, however, with large S.D. values. Hence, although these compounds may be used as substrates for BSEP or MRP2, transport experiments will be difficult given the high variability found here, and we would therefore rather conclude that they are not transported.

Discussion

The aim of the present study was to thoroughly test the impact of BS side-chain modifications with small fluorophores on the interaction with hepatocellular organic anion transporters, both with respect to inhibition and as potential substrates. The main findings are that firstly, all tested uptake

TABLE 2

Inhibition of uptake transporters by fluorescent bile acid derivatives

Transport experiments were performed as described in *Material and Methods*. The following substrates were used: NTCP, OATP1B3: 5 µM taurocholate; ASBT: 1 µM taurocholate; and OATP1B1 and OATP2B1: 1 µM estrone-3-sulfate. Transport was measured for 40 seconds. Substrate uptake values in % were corrected for uptake into WT CHO cells. Uptake in the absence of inhibitor was set to 100%. Results are the mean from two to four independent experiments with three technical replicates.

Compound	[I]	NTCP	OATP1B1	OATP1B3	OATP2B1	ASBT
	µM					
CenNBD	0	100	100	100	100	100
	0.1	98.5	101	108	90.9	95.8
	1	108.3	95.1	83.0	76.6	86.5
	10	38.7	64.9	26.6	23.0	76.4
	100	4.9	9.4	22.9	3.6	64.2
CenDNS	0	100	100	100	100	100
	0.1	85.9	98.8	82.7	94.0	85.5
	1	49.1	89.2	57.0	55.5	80.1
	10	7.8	30.4	13.0	11.5	59.4
	100	2.4	16.5	41.7	7.4	47.9
CenPB	0	100	100	100	100	100
	0.1	93.8	98.7	69.0	95.4	47.7
	1	73.9	93.7	62.0	89.8	40.4
	10	28.9	72.7	28.6	55.0	50.4
	100	5.8	51.2	19.0	15.7	51.0
CDCenNBD	0	100	100	100	100	100
	0.1	85.6	99.7	132	86.3	99.1
	1	67.5	95.6	95.5	85.4	108
	10	15.7	90.8	34.1	64.7	113
	100	17.7	86.8	41.2	66.9	91.7
CDCenDNS	0	100	100	100	100	100
	0.1	92.9	99.8	83.0	87.8	68.9
	1	61.8	94.3	64.0	87.9	123
	10	46.6	83.3	55.9	73.0	164
	100	46.2	84.0	50.5	62.7	109
CDCenPB	0	100	100	100	100	100
	0.1	64.5	91.9	56.7	98.0	43.4
	1	29.6	71.5	37.5	60.5	42.3
	10	6.7	36.3	28.8	13.2	48.6
	100	3.9	3.1	19.8	3.7	45.3
AcenNBD	0	100	100	100	100	100
	0.1	75.8	93.2	87.5	83.0	79.0
	1	87.6	89.4	103	86.7	98.8
	10	118	86.3	103	83.7	100
	100	75.8	78.3	88.4	49.1	144
AcenDNS	0	100	100	100	100	100
	0.1	92.7	99.6	109	95.8	82.0
	1	110	94.8	102	95.7	92.2
	10	120	93.5	94.8	114	99.6
	100	80.2	90.8	69.9	147	101
AcenPB	0	ND	100	100	100	ND
	0.1	ND	99.7	81.3	99.2	ND
	1	ND	96.8	63.8	96.4	ND
	10	ND	96.1	62.5	94.3	ND
	100	ND	89.0	62.5	68.8	ND

ND, not determined.

transporters are inhibited by at least one novel bile acid derivative (Table 2), whereby the interaction with ASBT was more restricted than interaction with other transporters. Secondly, neither NTCP (with the exception of a low transport activity for **CenDNS**) nor ASBT transport fluorescent BS derivatives, whereas all investigated OATPs accept more than one derivative (Table 4). Thirdly, the efflux transporter BSEP is subject to inhibition by all fluorescent bile acid derivatives, whereas MRP2 is not inhibited but rather stimulated in some instances (Table 3). Fourthly, efflux transport activity of the new BS derivatives is, as compared with the uptake transporters, very restricted (Table 5).

Given that, in particular, OATPs (Stieger and Hagenbuch, 2014) as well as MRP2 (van der Schoor et al., 2015) have a very broad substrate specificity and both are able transporting fluorescent dyes (Cantz et al., 2000; Brouwer et al., 2013;

TABLE 3

Inhibition of efflux transporters by fluorescent bile acid derivatives

Transport experiments were performed as described in *Material and Methods*. The following substrates were used: BSEP 2 μM taurocholate and MRP2 10 μM estradiol 17β-D-glucuronide. Transport was measured for 5 minutes. Substrate uptake values in % were corrected for transport in the absence of ATP, and uptake in the absence of inhibitor was set to 100%. Results are the mean from two to four independent experiments with three technical replicates.

Compound	[I]	BSEP	MRP2
	μM		
CenNBD	0	100	100
	1	87.5	94.5
	10	46.0	124
	100	12.0	140
CenDNS	0	100	100
	1	82.0	78.5
	10	50.5	106
	100	6.0	152
CenPB	0	100	100
	1	80.0	94.5
	10	58.0	94.5
	100	16.5	91.0
CDCenNBD	0	100	100
	1	67.5	122
	10	40.5	151
	100	6.5	228
CDCenDNS	0	100	100
	1	85.5	115
	10	43.0	132
	100	25.5	179
CDCenPB	0	100	100
	1	61.5	107
	10	13.0	151
	100	0.5	59.3
AcenNBD	0	100	100
	1	103	136
	10	97.5	132
	100	94.5	145
AcenDNS	0	100	100
	1	96.5	139
	10	97.0	136
	100	87.5	151
AcenPB	0	100	100
	1	116	99
	10	108	95
	100	102	93

Not one of these fluorophores was found to be a substrate. Using the molecules as inhibitors, **AcenNB** weakly interacted with OATP2B1, whereas **AcenPB** and **AcenDNS** weakly inhibited OATP1B3. This interaction is not surprising, as different fluorescent molecules have been shown to be transported by OATPs (Patik et al., 2015, 2018). In contrast, **AcenDNS** exhibited stimulation of OATP2B1 activity at high concentration. A stimulation of OATP2B1 transport activity by small molecules has been reported for prostaglandins (Pizzagalli et al., 2003) or steroids (Grube et al., 2006), but such stimulation is not restricted to OATP2B1 (Stieger and Hagenbuch, 2014). All fluorescent bile acid derivatives interacted with the tested transporters. As all of these uptake transporters are bile salt and bile acid transporters, we conclude that coupling of fluorophores to the side chain does not prevent the final probes from interacting with the respective bile acid binding sites on the transporters. Notably, **CDCenDNS** tended to transiently stimulate the transport activity of ASBT. This, to our knowledge, is a new finding, and a similar observation was made for silibinin for the low-affinity binding site of OATP1B1 (Wlcek et al., 2013). The truncated fluorescent probes did not interact with BSEP, but **AcenNBD** and **AcenDNS** were able to stimulate the transport activity of MRP2. A stimulation of the transport activity of MRP2 has also been reported for bosentan (Mano et al., 2007) and other selected drugs (Lagas et al., 2009; Gilibili et al., 2018).

In essence, neither NTCP nor ASBT transported any of the tested substrates. However, it cannot be concluded from this finding that modification of the side chain prevents bile salts to be substrates of NTCP. Since endogenous conjugation of taurine as well as glycine to the side chain of bile acids is via amide bond, we also coupled the fluorescent dyes to the side chain by an amide bond in the present work, similarly to an earlier study (Maglova et al., 1995). These authors report that two different side-chain derivatives of cholate were taken up in part in a sodium-dependent manner into primary rat hepatocytes, whereas an identical side-chain derivative of chenodeoxycholate displayed no dependence on sodium (Maglova et al., 1995). A fluorescein side-chain derivative of glycocholate was shown to be imported into rat hepatocytes in a sodium-dependent manner, indicating transport by rat NTCP (Grüne et al., 1996). On the other hand, a lysyl-fluorescein side-chain derivative of cholate was not transported by NTCP (de Waart et al., 2010). A fluorescent side-chain derivative of cholate has previously been shown to be transported by

Patik et al., 2015), special care was taken to separate the desired reaction products (fluorescent bile acid conjugates) with great purity from the fluorescent dye starting materials after the synthetic coupling reactions. As an additional control, possible interactions of the fluorescent dyes with the investigated transporters were probed. To this end, bile acid–truncated fluorescent probes **AcenNBD**, **AcenDNS**, and **AcenPB** were tested as potential inhibitors and substrates.

TABLE 4

Transport of fluorescent bile acid derivatives by uptake transporters

Transport experiments were performed as described in *Material and Methods*. The substrate conc. were 5 μM, and transport was measured for 5 minutes. Uptake values were corrected for uptake into WT CHO cells. Results are given in picomole per milligram protein $\times$ 5 minutes. Data are mean $\pm$ S.D. from two to four independent experiments with three technical replicates.

Compound	NTCP	OATP1B1	OATP1B3	OATP2B1	ASBT
CenNBD	NT	67.0 $\pm$ 30.0	NT	26.1 $\pm$ 13.7	NT
CenDNS	20.3 $\pm$ 10.0	NT	1577 $\pm$ 509	175 $\pm$ 20.2	NT
CenPB	NT	21.6 $\pm$ 13.1	306 $\pm$ 188	NT	NT
CDCenNBD	NT	908 $\pm$ 309	8545 $\pm$ 3200	1779 $\pm$ 405	NT
CDCenDNS	NT	NT	1524 $\pm$ 311	141 $\pm$ 26.61	NT
CDCenPB	NT	NT	162 $\pm$ 59.7	60.5 $\pm$ 18.4	NT
AcenNBD	NT	NT	NT	NT	NT
AcenDNS	NT	NT	NT	NT	NT
AcenPB	ND	NT	NT	NT	ND

ND, not determined; NT, no transport.

TABLE 5

Transport of fluorescent bile acid derivatives by efflux transporters

Transport experiments were performed as described in *Material and Methods*. The substrate conc. were 5 μM, and transport was measured for 5 minutes. Uptake values were corrected for uptake in the absence of ATP. Results are given in picomole per milligram protein × 5 minutes. Data are mean ± S.D. from two to four independent experiments with three technical replicates.

Compound	BSEP	MRP2
CenNBD	NT	NT
CenDNS	NT	NT
CenPB	81.4 ± 75.1	NT
CDCenNBD	NT	NT
CDCenDNS	NT	NT
CDCenPB	115 ± 103	404 ± 355
AcenNBD	NT	NT
AcenDNS	NT	NT
AcenPB	NT	NT

NT, no transport.

heterologously expressed NTCP and rNTCP (De Bruyn et al., 2014). While developing fluorinated BS derivatives amenable to positron emission tomography studies, it was observed that a lithocholic acid derivative with a modified side chain was accepted by NTCP as substrate (Testa et al., 2017). Hence, based on the current literature, it is hard to predict the impact of side-chain modification of bile acids affecting their substrate properties for NTCP. It should be pointed out, however, that the substrate pattern of NTCP not only includes bile salts but also other organic anions as well as some drugs (Anwer and Stieger, 2014). It is interesting to note that a substrate pharmacophore for NTCP without consideration of the side chain has been presented (Greupink et al., 2012; Dong et al., 2015). There is a consensus that the substrate specificity of ASBT is much narrower than that of NTCP (Claro da Silva et al., 2013; Anwer and Stieger, 2014; Dawson and Karpen, 2015). In this context, the results for ASBT were not surprising.

Given the broad substrate specificity of OATPs, we expected that they would also transport some of our novel BS derivatives (Table 4). Here, it is interesting to note that OATP2B1 transports five out of the six tested fluorescent BS probes. This is in contrast with an earlier study, in which we found no transport of conjugated bile acids by OATP2B1 (Kullak-Ublick et al., 2001). It is, however, very reassuring that none of the fluorescent dyes we used was a substrate of the tested OATPs. Hence, these dyes might be coupled to different positions of the bile acid skeleton (Yamaguchi et al., 2006).

Given that a fluorescent side-chain derivative of bile salts was reported to be a BSEP substrate (Yamaguchi et al., 2010), it was somewhat unexpected that none of our derivatives was transported by BSEP. However, our data fit well with the concept that BSEP transports almost exclusively conjugated bile acids (Stieger, 2011). Although all derivatives were inhibitors of BSEP, none of the truncated fluorescent probes significantly interacted with this transporter. Although MRP2 transports a wide variety of endogenous metabolites as well as drug and xenobiotic metabolites (Keppler, 2011), none of our bile acid derivatives was a good substrate. This is interesting in view of the fact that some of our derivatives were able to stimulate transport activity of a prototypical substrate of MRP2. This may, at least in part, be explained by the rather complex transport kinetics of MRP2 (Guyot et al., 2014). Again, none of the fluorescent dyes used here was transported by MRP2. However, it should be kept in mind that extrapolation of driving forces from in vitro systems to in vivo

situations is very difficult at best. It can therefore not be excluded that in an in vivo model **CDCenPB** might be taken up into a liver system and secreted into bile. As it is possible to keep livers with continuous perfusion alive out of bodies for up to a week now (Eshmuminov et al., 2020, 2021), **CDCenPB** for instance could be evaluated as a dynamic liver function marker in ex situ perfused (human) livers.

In conclusion, side-chain modification of bile acids does not prevent the conjugates interacting with organic anion and bile salt uptake and efflux transporters. However, the new fluorescent compounds are not transport substrates for bile acid uptake transporters NCTP and ASBT. Furthermore, with the exception of **CDCenPB**, they are not transported by the canalicular efflux transporters and thus are not suitable for in vivo studies. Nevertheless, these new fluorescent BS derivatives have some potential as imaging agents if substrate uptake into hepatocytes or cells is to be followed. Since **CDCenPB** may be both a substrate of the uptake transporters OATP1B3 and OATP2B1 as well as of the canalicular efflux transporters BSEP and MRP2, future studies in in vivo models of bile formation with this compound are warranted.

Authorship Contributions

Participated in research design: Leuenberger, Häusler, Stieger, Lochner.

Conducted experiments: Leuenberger, Häusler, Höhn, Euler.

Contributed new reagents or analytic tools: Leuenberger.

Performed data analysis: Leuenberger, Häusler, Stieger, Lochner.

Wrote or contributed to the writing of the manuscript: Leuenberger, Stieger, Lochner.

References

Aithal GP, Watkins PB, Andrade RJ, Larrey D, Molokhia M, Takikawa H, Hunt CM, Wilke RA, Avigan M, Kaplowitz N, et al. (2011) Case definition and phenotype standardization in drug-induced liver injury. *Clin Pharmacol Ther* **89**:806–815.
Anwer MS and Stieger B (2014) Sodium-dependent bile salt transporters of the SLC10A transporter family: more than solute transporters. *Pflugers Arch* **466**: 77–89.
Brouwer KL, Keppler D, Hoffmaster KA, Bow DA, Cheng Y, Lai Y, Palm JE, Stieger B, and Evers R; International Transporter Consortium (2013) In vitro methods to support transporter evaluation in drug discovery and development [published correction appears in *Clin Pharmacol Ther* (2013) 94:412]. *Clin Pharmacol Ther* **94**: 95–112.
Bull LN and Thompson RJ (2018) Progressive familial intrahepatic cholestasis. *Clin Liver Dis* **22**:657–669.
Cantz T, Nies AT, Brom M, Hofmann AF, and Keppler D (2000) MRP2, a human conjugate export pump, is present and transports fluo 3 into apical vacuoles of Hep G2 cells. *Am J Physiol Gastrointest Liver Physiol* **278**:G522–G531.
Cieslak KP, Baur O, Verheij J, Bennink RJ, and van Gulik TM (2016) Liver function declines with increased age. *HPB (Oxford)* **18**:691–696.
Claro da Silva T, Polli JE, and Swaan PW (2013) The solute carrier family 10 (SLC10): beyond bile acid transport. *Mol Aspects Med* **34**:252–269.
Corsini A and Bortolini M (2013) Drug-induced liver injury: the role of drug metabolism and transport. *J Clin Pharmacol* **53**:463–474.
Craddock AL, Love MW, Daniel RW, Kirby LC, Walters HC, Wong MH, and Dawson PA (1998) Expression and transport properties of the human ileal and renal sodium-dependent bile acid transporter. *Am J Physiol* **274**:G157–G169.
Dawson PA and Karpen SJ (2015) Intestinal transport and metabolism of bile acids. *J Lipid Res* **56**:1085–1099.
De Bruyn T, Fattah S, Stieger B, Augustijns P, and Annaert P (2011) Sodium fluorescein is a probe substrate for hepatic drug transport mediated by OATP1B1 and OATP1B3. *J Pharm Sci* **100**:5018–5030.
De Bruyn T, Sempels W, Snoeys J, Holmstock N, Chatterjee S, Stieger B, Augustijns P, Hofkens J, Mizuno H, and Annaert P (2014) Confocal imaging with a fluorescent bile acid analogue closely mimicking hepatic taurocholate disposition. *J Pharm Sci* **103**:1872–1881.
de Waart DR, Häusler S, Vlaming ML, Kunne C, Hänggi E, Gruss HJ, Oude Elferink RP, and Stieger B (2010) Hepatic transport mechanisms of cholyl-L-lysyl-fluorescein. *J Pharmacol Exp Ther* **334**:78–86.

de Waart DR, Paulusma CC, Kunne C, and Oude Elferink RP (2006) Multidrug resistance associated protein 2 mediates transport of prostaglandin E2. *Liver Int* **26**:362–368.

Dong Z, Ekins S, and Polli JE (2015) A substrate pharmacophore for the human sodium taurocholate co-transporting polypeptide. *Int J Pharm* **478**:88–95.

Eshmuminov D, Becker D, Bautista Borrego L, Hefti M, Schuler MJ, Hagedorn C, Muller X, Mueller M, Onder C, Graf R, et al. (2020) An integrated perfusion machine preserves injured human livers for 1 week. *Nat Biotechnol* **38**:189–198.

Eshmuminov D, Schuler MJ, Becker D, Bautista Borrego L, Mueller M, Hagedorn C, Häusler S, Steiger J, Tibbitt MW, Dutkowski P, et al. (2021) Bile formation in long-term ex situ perfused livers. *Surgery* **169**:894–902 DOI: 10.1016/j.surg.2020.11.042.

Esteller A (2008) Physiology of bile secretion. *World J Gastroenterol* **14**:5641–5649.

Frosch B and Wagener H (1967) Quantitative determination of conjugated bile acids in serum in acute hepatitis. *Nature* **213**:404–405.

Gerloff T, Stieger B, Hagenbuch B, Madon J, Landmann L, Roth J, Hofmann AF, and Meier PJ (1998) The sister of P-glycoprotein represents the canalicular bile salt export pump of mammalian liver. *J Biol Chem* **273**:10046–10050.

Gilibili RR, Kurawattimath V, Murali BV, Lai Y, Mariappan TT, Shen H, and Chatterjee S (2018) In vitro stimulation of multidrug resistance-associated protein 2 function is not reproduced in vivo in rats. *Pharmaceutics* **10**:125.

Greupink R, Nabuurs SB, Zarzycka B, Verweij V, Monshouwer M, Huisman MT, and Russel FG (2012) In silico identification of potential cholestasis-inducing agents via modeling of Na(+)-dependent taurocholate cotransporting polypeptide substrate specificity. *Toxicol Sci* **129**:35–48.

Grube M, Köck K, Karner S, Reuther S, Ritter CA, Jedlitschky G, and Kroemer HK (2006) Modification of OATP2B1-mediated transport by steroid hormones. *Mol Pharmacol* **70**:1735–1741.

Grüne S, Meng XJ, and Weinman SA (1996) cAMP stimulates fluorescent bile acid uptake into hepatocytes by membrane hyperpolarization. *Am J Physiol* **270**:G339–G346.

Gui C, Miao Y, Thompson L, Wahlgren B, Mock M, Stieger B, and Hagenbuch B (2008) Effect of pregnane X receptor ligands on transport mediated by human OATP1B1 and OATP1B3. *Eur J Pharmacol* **584**:57–65.

Guyot C, Hofstetter L, and Stieger B (2014) Differential effects of membrane cholesterol content on the transport activity of multidrug resistance-associated protein 2 (ABCC2) and of the bile salt export pump (ABCB11). *Mol Pharmacol* **85**:909–920.

Hagenbuch B and Stieger B (2013) The SLCO (former SLC21) superfamily of transporters. *Mol Aspects Med* **34**:396–412.

Halilbasic E, Claudel T, and Trauner M (2013) Bile acid transporters and regulatory nuclear receptors in the liver and beyond. *J Hepatol* **58**:155–168.

Hoekstra LT, de Graaf W, Nibourg GAA, Heger M, Bennink RJ, Stieger B, and van Gulik TM (2013) Physiological and biochemical basis of clinical liver function tests: a review. *Ann Surg* **257**:27–36.

Holzinger F, Schteingart CD, Ton-Nu H-T, Cerrè C, Steinbach JH, Yeh H-Z, and Hofmann AF (1998) Transport of fluorescent bile acids by the isolated perfused rat liver: kinetics, sequestration, and mobilization. *Hepatology* **28**:510–520.

Holzinger F, Schteingart CD, Ton-Nu HT, Eming SA, Monte MJ, Hagey LR, and Hofmann AF (1997) Fluorescent bile acid derivatives: relationship between chemical structure and hepatic and intestinal transport in the rat. *Hepatology* **26**:1263–1271.

Huber RD, Gao B, Sidler Pfändler MA, Zhang-Fu W, Leuthold S, Hagenbuch B, Folkers G, Meier PJ, and Stieger B (2007) Characterization of two splice variants of human organic anion transporting polypeptide 3A1 isolated from human brain. *Am J Physiol Cell Physiol* **292**:C795–C806.

Keppler D (2011) Multidrug resistance proteins (MRPs, ABCCs): importance for pathophysiology and drug therapy. *Handb Exp Pharmacol* **201**:299–323 Available from: 10.1007/978-3-642-14541-4_8.

Kjærgaard K, Frisch K, Sørensen M, Munk OL, Hofmann AF, Horsager J, Schacht AC, Erickson M, Shapiro D, and Keiding S (2021) Obeticholic acid improves hepatic bile acid excretion in patients with primary biliary cholangitis. *J Hepatol* **74**:58–65.

Kullak-Ublick GA, Ismair MG, Stieger B, Landmann L, Huber R, Pizzagalli F, Fattinger K, Meier PJ, and Hagenbuch B (2001) Organic anion-transporting polypeptide B (OATP-B) and its functional comparison with three other OATPs of human liver. *Gastroenterology* **120**:525–533.

Lagas JS, van der Kruijssen CM, van de Wetering K, Beijnen JH, and Schinkel AH (2009) Transport of diclofenac by breast cancer resistance protein (ABCG2) and stimulation of multidrug resistance protein 2 (ABCC2)-mediated drug transport by diclofenac and benzbromarone. *Drug Metab Dispos* **37**:129–136.

LaRusso NF, Hoffman NE, Hofmann AF, and Korman MG (1975) Validity and sensitivity of an intravenous bile acid tolerance test in patients with liver disease. *N Engl J Med* **292**:1209–1214.

Maglova LM, Jackson AM, Meng XJ, Carruth MW, Schteingart CD, Ton-Nu HT, Hofmann AF, and Weinman SA (1995) Transport characteristics of three fluorescent conjugated bile acid analogs in isolated rat hepatocytes and couplets. *Hepatology* **22**:637–647.

Mahdi ZM, Synal-Hermanns U, Yoker A, Locher KP, and Stieger B (2016) Role of multidrug resistance protein 3 in antifungal-induced cholestasis. *Mol Pharmacol* **90**:23–34.

Mano Y, Usui T, and Kamimura H (2007) Substrate-dependent modulation of UDP-glucuronosyltransferase 1A1 (UGT1A1) by propofol in recombinant human UGT1A1 and human liver microsomes. *Basic Clin Pharmacol Toxicol* **101**:211–214.

Milkiewicz P, Saksena S, Cardenas T, Mills CO, and Elias E (2000) Plasma elimination of cholyl-lysyl-fluorescein (CLF): a pilot study in patients with liver cirrhosis. *Liver* **20**:330–334.

Noé J, Stieger B, and Meier PJ (2002) Functional expression of the canalicular bile salt export pump of human liver. *Gastroenterology* **123**:1659–1666.

Obaidat A, Roth M, and Hagenbuch B (2012) The expression and function of organic anion transporting polypeptides in normal tissues and in cancer. *Annu Rev Pharmacol Toxicol* **52**:135–151.

Palermo DP, DeGraaf ME, Marotti KR, Rehberg E, and Post LE (1991) Production of analytical quantities of recombinant proteins in Chinese hamster ovary cells using sodium butyrate to elevate gene expression. *J Biotechnol* **19**:35–47.

Patik I, Kovacsics D, Német O, Gera M, Várady G, Stieger B, Hagenbuch B, Szakács G, and Özvegy-Laczka C (2015) Functional expression of the 11 human Organic Anion Transporting Polypeptides in insect cells reveals that sodium fluorescein is a general OATP substrate. *Biochem Pharmacol* **98**:649–658.

Patik I, Székely V, Német O, Szepesi Á, Kucsma N, Várady G, Szakács G, Bakos É, and Özvegy-Laczka C (2018) Identification of novel cell-impermeant fluorescent substrates for testing the function and drug interaction of Organic Anion-Transporting Polypeptides, OATP1B1/1B3 and 2B1. *Sci Rep* **8**:2630.

Paumgartner G, Vasella DL, Herz R, Reichen J, and Preisig R (1979) [Hepatic extraction of taurocholate and indocyanine green in patients with liver disease (author's transl)]. *Z Gastroenterol* **17**:753–761.

Pizzagalli F, Varga Z, Huber RD, Folkers G, Meier PJ, and St-Pierre MV (2003) Identification of steroid sulfate transport processes in the human mammary gland. *J Clin Endocrinol Metab* **88**:3902–3912.

Pollheimer MJ, Fickert P, and Stieger B (2014) Chronic cholestatic liver diseases: clues from histopathology for pathogenesis. *Mol Aspects Med* **37**:35–56.

Rais R, Acharya C, Mackerell AD, and Polli JE (2010) Structural determinants for transport across the intestinal bile acid transporter using C-24 bile acid conjugates. *Mol Pharm* **7**:2240–2254.

Sakka SG (2018) Assessment of liver perfusion and function by indocyanine green in the perioperative setting and in critically ill patients. *J Clin Monit Comput* **32**:787–796.

Selvapatt N, Singanayagam A, Wendon J, and Antoniades CG (2014) Understanding infection susceptibility in patients with acute-on-chronic liver failure. *Intensive Care Med* **40**:1363–1366.

Smith PK, Krohn RI, Hermanson GT, Mallia AK, Gartner FH, Provenzano MD, Fujimoto EK, Goeke NM, Olson BJ, and Klenk DC (1985) Measurement of protein using bicinchoninic acid. *Anal Biochem* **150**:76–85.

Stieger B (2011) The role of the sodium-taurocholate cotransporting polypeptide (NTCP) and of the bile salt export pump (BSEP) in physiology and pathophysiology of bile formation. *Handb Exp Pharmacol* **201**:205–259.

Stieger B and Hagenbuch B (2014) Organic anion-transporting polypeptides. *Curr Top Membr* **73**:205–232.

Stieger B, Heger M, de Graaf W, Paumgartner G, and van Gulik T (2012) The emerging role of transport systems in liver function tests. *Eur J Pharmacol* **675**:1–5.

Testa A, Dall'Angelo S, Mingarelli M, Augello A, Schweiger L, Welch A, Elmore CS, Sharma P, and Zanda M (2017) Design, synthesis, in vitro characterization and preliminary imaging studies on fluorinated bile acid derivatives as PET tracers to study hepatic transporters. *Bioorg Med Chem* **25**:963–976.

Treiber A, Schneiter R, Häusler S, and Stieger B (2007) Bosentan is a substrate of human OATP1B1 and OATP1B3: inhibition of hepatic uptake as the common mechanism of its interactions with cyclosporin A, rifampicin, and sildenafil. *Drug Metab Dispos* **35**:1400–1407.

van der Schoor LW, Verkade HJ, Kuipers F, and Jonker JW (2015) New insights in the biology of ABC transporters ABCC2 and ABCC3: impact on drug disposition. *Expert Opin Drug Metab Toxicol* **11**:273–293.

Wlcek K, Koller F, Ferenci P, and Stieger B (2013) Hepatocellular organic anion-transporting polypeptides (OATPs) and multidrug resistance-associated protein 2 (MRP2) are inhibited by silibinin. *Drug Metab Dispos* **41**:1522–1528.

Yamaguchi H, Okada M, Akitaya S, Ohara H, Mikkaichi T, Ishikawa H, Sato M, Matsuura M, Saga T, Unno M, et al. (2006) Transport of fluorescent chenodeoxycholic acid via the human organic anion transporters OATP1B1 and OATP1B3. *J Lipid Res* **47**:1196–1202.

Yamaguchi K, Murai T, Yabuuchi H, Hui SP, and Kurosawa T (2010) Measurement of bile salt export pump transport activities using a fluorescent bile acid derivative. *Drug Metab Pharmacokinet* **25**:214–219.

Zhao W, Zitzow JD, Ehresman DJ, Chang SC, Butenhoff JL, Forster J, and Hagenbuch B (2015) Na+/taurocholate cotransporting polypeptide and apical sodium-dependent bile acid transporter are involved in the disposition of perfluoroalkyl sulfonates in humans and rats. *Toxicol Sci* **146**:363–373.

Address correspondence to: Martin Lochner, Institute of Biochemistry and Molecular Medicine, University of Bern, Bühlstrasse 28, 3012 Bern, Switzerland. E-mail: martin.lochner@ibmm.unibe.ch; or Bruno Stieger, Department of Clinical Pharmacology and Toxicology, University Hospital Zürich, Rämistrasse 100, 8091 Zürich, Switzerland. E-mail: bruno.stieger@uzh.ch